Supplementary Material for

Extreme melt events on northern James Ross Island, Antarctic Peninsula region, linked to isentropic drawdown and foehn winds: multi-scale analysis using in-situ observations and the Weather Research and Forecasting model simulations

Matějka Michael[1], Láska Kamil[1], Stachoň Zdeněk[1]

[1] Department of Geography, Faculty of Science, Masaryk University, Kotlářská 2, 611 37 Brno, Czech Republic

Corresponding author: Michael Matějka (matejkamichael@mail.muni.cz)

Contents of this file

Table S1
Figures S1 to S9

Introduction

This supporting information contains a table with detailed WRF model configuration (Table S1) and nine figures S1 to S9. These figures provide further information about the Nov 22 and Jan 23 ablations events and a satellite imagery for the Dec 22 event.

WRF model configuration

Table S1. WRF model domains, time step and physics configuration

Parameter	Value
Domain D01 size and resolution	164 × 129 grid points, 8.1 km
Domain D02 size and resolution	142 × 142 grid points, 2.7 km
Domain D03 size and resolution	202 × 202 grid points, 0.7 km
Domain D04 size and resolution	157 × 154 grid points, 0.3 km
Number of vertical levels	65 levels, the lowest one (for air temperature) at ~7 m a.g.l.
Time step	adaptive; 9–45 s [D01], 3–15 s [D02], 1–5 s [D03], 0.3–1.5 s [D04]
Microphysics scheme	Thompson [Thompson and other, 2008]
Shortwave radiation	RRTMG [Iacono and others, 2008]

Longwave radiation	RRTMG[Iacono and others, 2008]
Convection scheme	turned off [all domains]
Land surface model	NoahMP [Niu and others, 2011]
Boundary layer scheme	3D TKE [Zhang and others, 2018]
Surface layer scheme	MYNN [Nakanishi, Niino, 2006]
Fractional_seaice	Activated
Sea ice thickness option	Uniform
Sea ice thickness default value	1.2 m [following Kern and other, 2016]
Sea ice albedo	Variable
Snow on sea ice option	Bounded by limits
Snow on sea ice–minimum	0 m
Snow on sea ice–maximum	2 m

The ablation event 11 – 22 November 2023

The first period of pronounced surface melt on investigated glaciers during the summer season 2022/2023 developed in mid-November 2022 (Fig. S1). This event brought extensive periods of air temperatures above 0 °C to the Triangular Glacier, leading to a mean air temperature of 2.9 °C. The maximum air temperature of 8.1 °C was recorded on 15 November (Fig. S1). Davies Dome experienced generally cooler conditions, with a mean air temperature of 0.2 °C and a maximum of 4.7 °C. Wind speed was noticeably lower on a cirque-confined Triangular Glacier than on the well-ventilated Davies Dome, with a mean difference of 3.2 $m \cdot s^{-1}$. Davies Dome also experienced short spikes over 20 $m \cdot s^{-1}$. The observed net radiation on Triangular Glacier reached an average value of 81.4 $W \cdot m^{-2}$ while daily maximum values exceeded 400 $W \cdot m^{-2}$ (Fig. S1). In-situ net radiation observation was unavailable on Davies Dome; however, the WRF model outputs suggest that the modelled net radiation there was about 66 % lower than on Triangular Glacier (Fig. S1). The modelled sensible heat flux was often slightly positive at both sites (Fig. S2) with generally higher values on Triangular Glacier than on Davies Dome (average difference: 30.6 $W \cdot m^{-2}$). Conversely, the latent heat flux reached slightly more negative values on Davies Dome. This event was only moderate regarding surface ablation on Davies Dome, leading to a snowmelt of 45.9 mm w.e., whereas a significant total melt of 247.1 mm w.e. was observed on Triangular Glacier (Fig. S1). Importantly, the winter snow cover at this site melted completely on 16 November 2022,

leading to early-season ice ablation, which peaked on 22 November with a daily amount of 48.6 mm w.e.

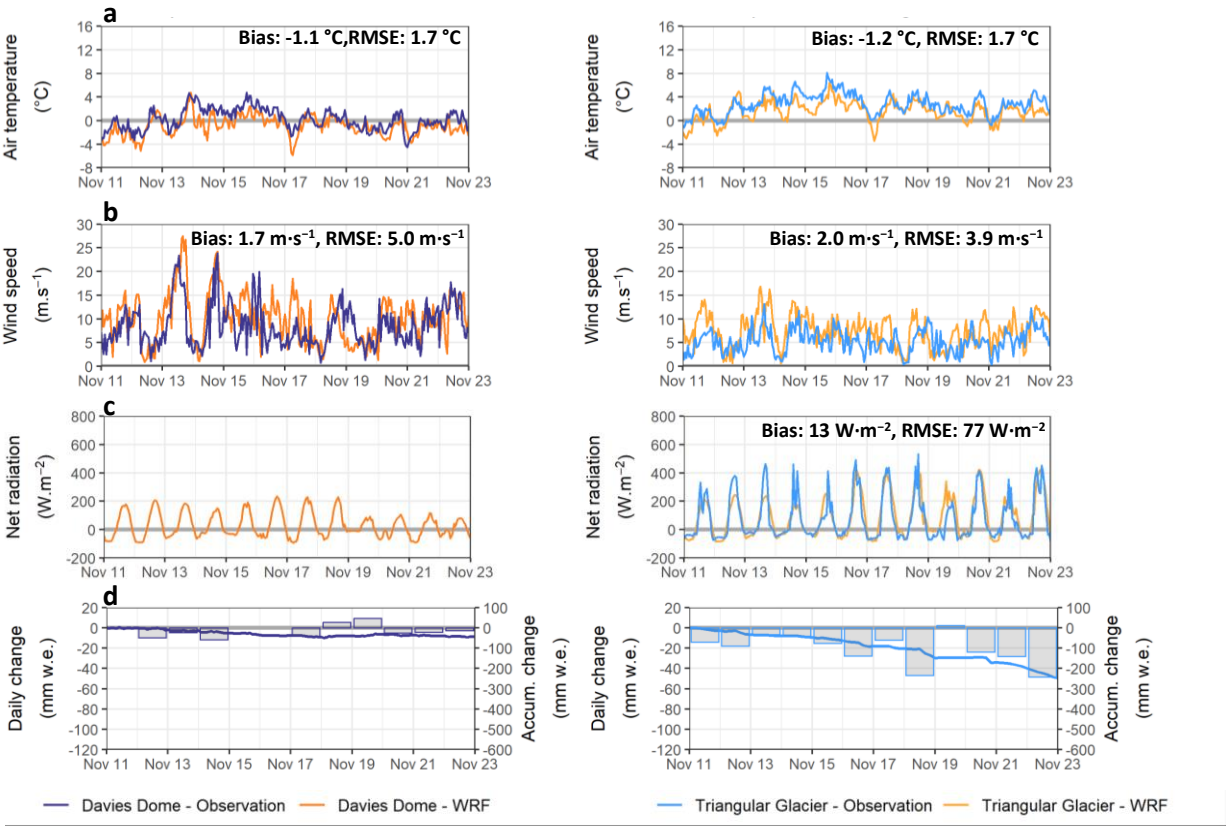

Figure S1. Observed and WRF-simulated near-surface meteorological parameters: air temperature (a), wind speed (b), net radiation (c),daily and cumulative surface height changes in mm w. e. (d) on Davies Dome (left) and Triangular Glacier (right) between 11 – 22 November 2022. Where available, the bias and root-mean-squared error (RMSE) of the WRF model are given in the plot.

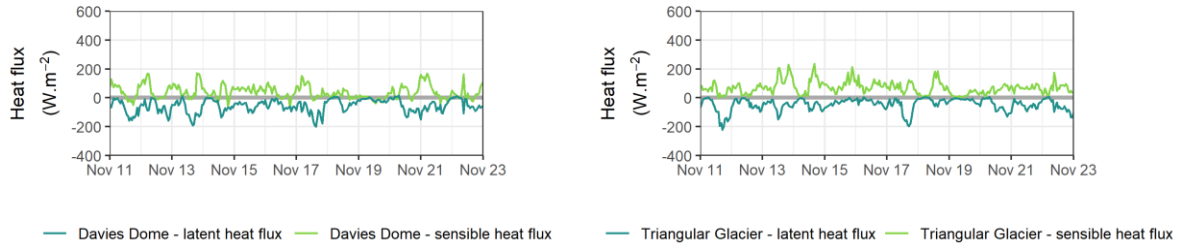

Figure S2. WRF-simulated sensible and latent heat fluxes on Davies Dome (left) and Triangular Glacier (right) between 11 – 22 November 2022.

The ablation event 05 – 15 January 2023

The third analysed period lasting between 05 – 15 January 2023 was slightly warmer than the *Dec 22* event at both sites. However, the mean ablation rate during the *Jan 23* event was reduced by moderate 26 % on Triangular Glacier compared to the *Dec 22* event, while on Davies Dome, the reduction was only 4 %. The highest air temperature during this event was observed on 09 January 2023 reaching 8.1 °C on Davies Dome and 10.3 °C on Triangular Glacier. Very high air temperatures coincided with elevated wind speed values on Davies Dome, reaching 23.2 $m \cdot s^{-1}$(Fig. S3). These conditions resemble the combination of extremely high air temperature and increased wind speed observed on 22 December 2022 (Fig. S3), the day with the most intense ablation within all investigated periods. The most intense daily mean ablation reached 33.9 mm w.e. on Davies Dome and 79.0 mm w.e. on Triangular Glacier, both on 09 January 2023. On the top of net radiation, strong melt on this day was supported by sensible heat flux reaching ≥200 $W \cdot m^{-2}$ for a large part of the day (Fig. S4).

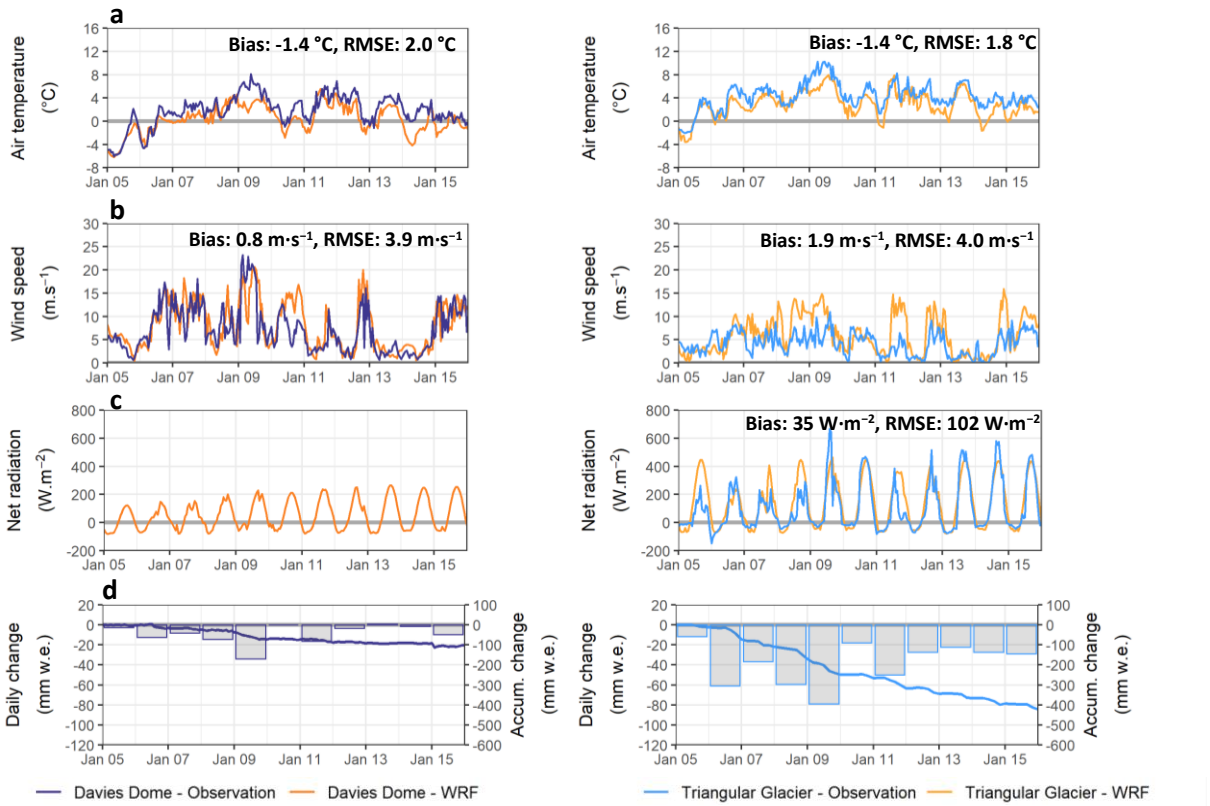

Figure S3. Observed and WRF-simulated near-surface meteorological parameters: air temperature (a), wind speed (b), net radiation (c), daily and cumulative surface height changes in mm w. e. (d) on Davies Dome (left) and Triangular Glacier (right) between 05 – 16 January 2023. Where available, the root-mean-squared error (RMSE) and bias of the WRF model are given in the plot.

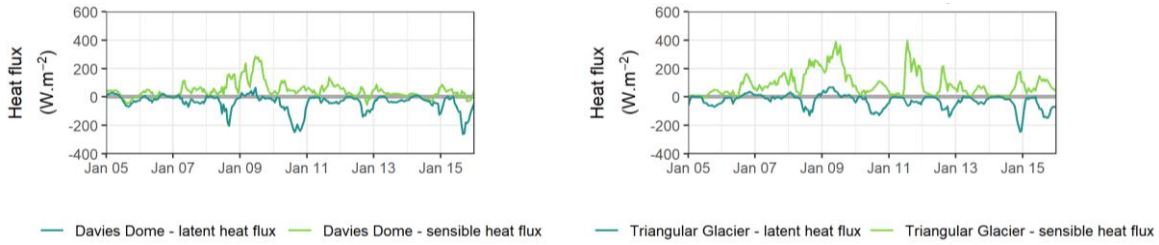

Figure S4. WRF-simulated sensible and latent heat fluxes on Davies Dome (left) and Triangular Glacier (right) between 05 – 16 January 2023.

Synoptic- and meso-scale processes leading to significant glacier ablation during Nov 22 and Jan 23 events

The figures S5 to S8 provide further details about the synoptic- and mesoscale processes during culmination phases of the Nov 22 and Jan 23 ablations events analogically to the Fig. 6 and Fig. 7 which describes the culmination phase of the Dec 22 event. Both Figs. S6 and S8 show signs of foehn occurrence: leeward warming, isentropic drawdown, relative humidity reduction and downward motion easterly from the leading Antarctic Peninsula ridge.

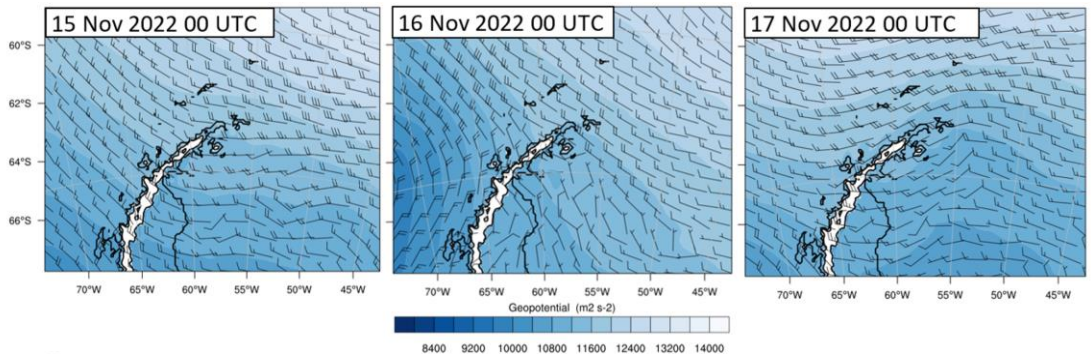

Figure S5. WRF-simulated 850-hPa wind vectors and geopotential over the Antarctic Peninsula region from 15 to 17 November 2022.

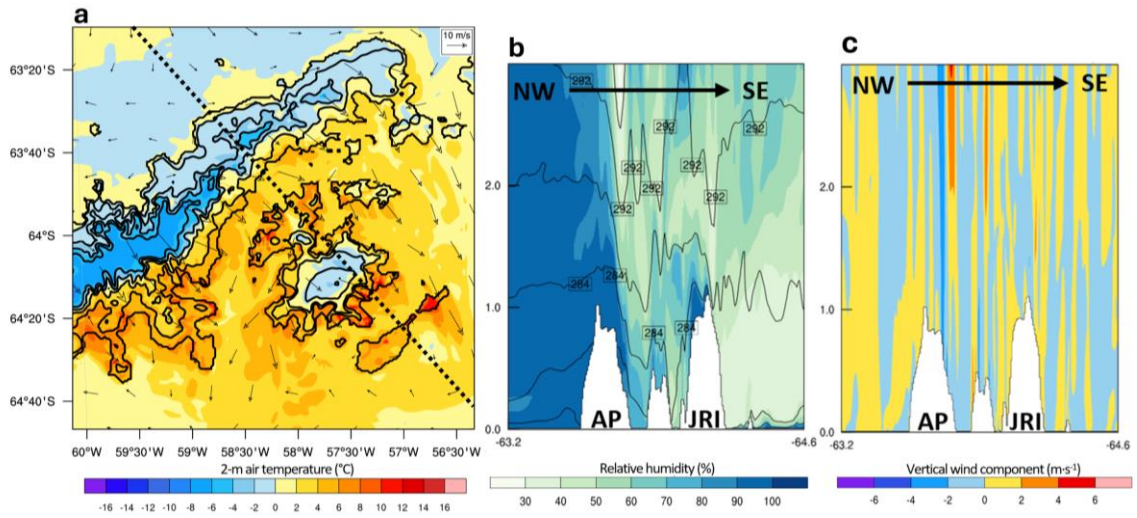

Figure S6. WRF-simulated 2-m air temperature (color), 10-m wind speed (arrows), and contours of model terrain at 400-m interval (black lines) in the northern Antarctic Peninsula region (**a**). Vertical cross-sections of relative humidity and potential temperature in NW-SE direction (**b**) the same for vertical wind component (**c**). The position of the cross-section is shown as a dotted line in section **a**. The horizontal arrows in the upper part of the cross-sections indicate the prevailing flow direction. The outputs are valid for the culmination phase of the ablation event on 15 November 2022 at 17 UTC. The 'z-wind component' is the vertical component of the wind vector.

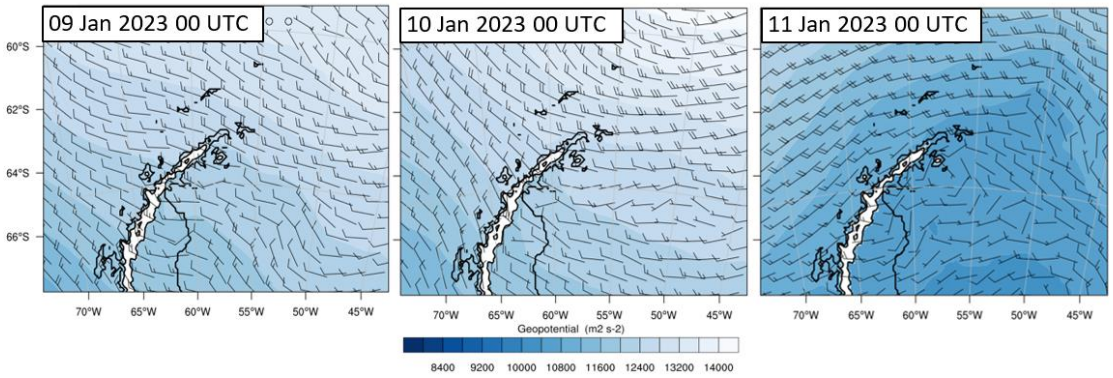

Figure S7. WRF-simulated 850-hPa wind vectors and geopotential over the Antarctic Peninsula region from 08 to 10 January 2023.

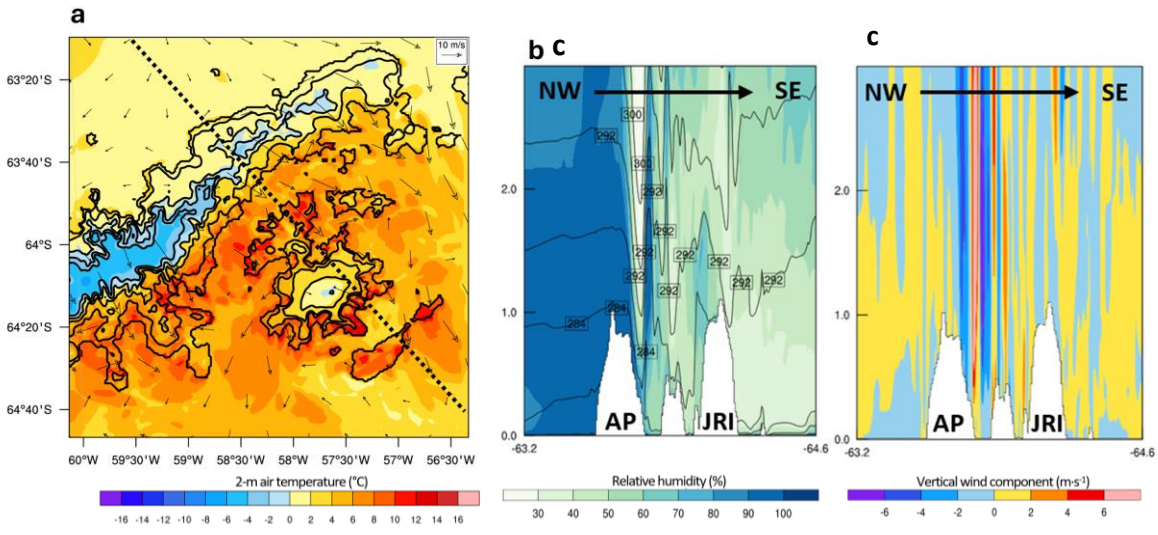

Figure S8. WRF-simulated 2-m air temperature (color), 10-m wind speed (arrows), and contours of model terrain at 400-m interval (black lines) in the northern Antarctic Peninsula region (**a**). Vertical cross-sections of relative humidity and potential temperature in NW-SE direction (**b**) the same for vertical wind component (**c**). The position of the cross-section is shown as a dotted line in section **a**. The horizontal arrows in the upper part of the cross-sections indicate the prevailing flow direction. The outputs are valid for the culmination phase of the ablation event on 09 January 2023 at 11 UTC. The 'z-wind component' is the vertical component of the wind vector.

Satellite-based extent of snow cover melt

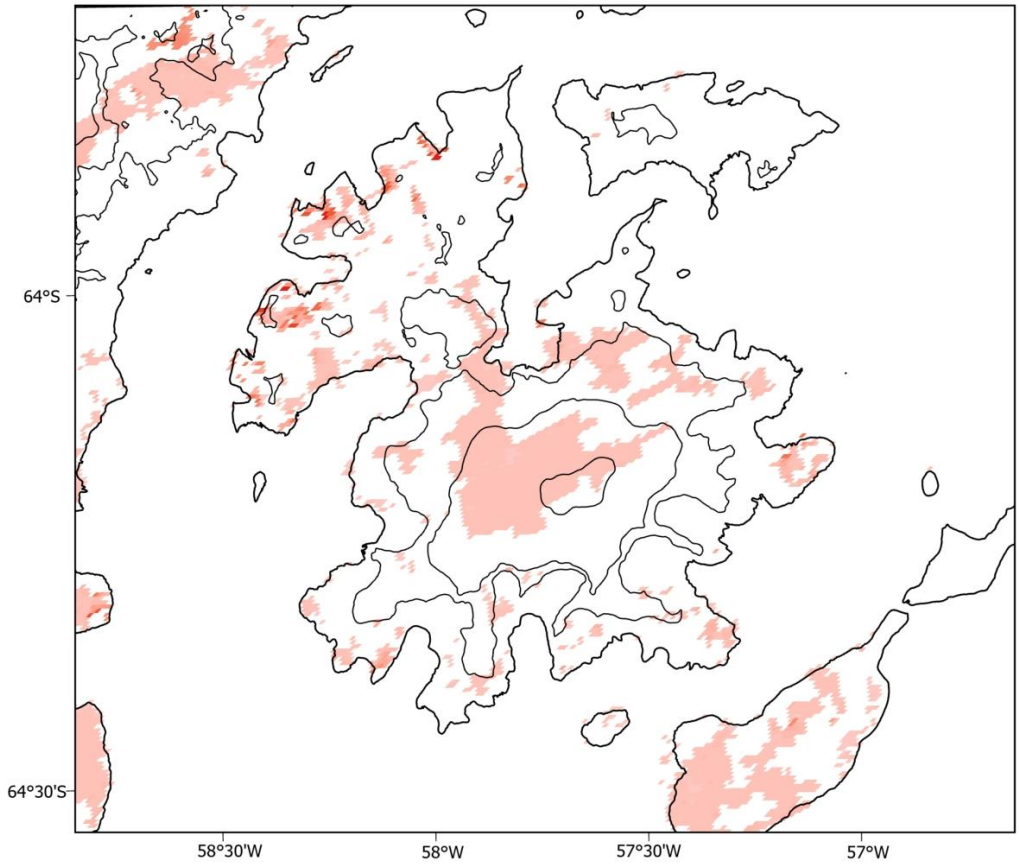

Figure S9. Areas with indicated snow cover melt (pink) in James Ross Island region between 15 December 2022 and 28 December 2022 using the MODIS/Aqua Snow Cover Daily L3 Global 500m SIN Grid product.